QKI dysregulation induces extensive splicing changes in T-cell acute lymphoblastic leukemia

Bruno Palhais,[1-4*] Nitesh D. Sharma,[5,6*] Igor Fijalkowski,[1,2,4] Tim Pieters,[1-4,7] Dieter Deforce,[2,8,9] Filip Van Nieuwerburgh,[2,8,9] Pieter Mestdagh,[1,2,10#] Panagiotis Ntziachristos,[1,2,4#] Ksenia Matlawska-Wasowska[5,6#] and Pieter Van Vlierberghe[1-3#†]

[1]Center for Medical Genetics, Ghent University and University Hospital, Ghent, Belgium; [2]Cancer Research Institute Ghent (CRIG), Ghent, Belgium; [3]Normal and Malignant Hematopoiesis Lab, Department of Biomolecular Medicine, Ghent University, Ghent, Belgium; [4]Leukemia Therapy Resistance Unit, Department of Biomolecular Medicine, Ghent University, Ghent, Belgium; [5]Department of Cell, Developmental and Integrative Biology, University of Alabama at Birmingham, Birmingham, AL, USA; [6]Department of Pediatrics, University of New Mexico, Albuquerque, NM, USA; [7]Unit for Translational Research in Oncology, Department of Diagnostic Sciences, Ghent University, Ghent, Belgium; [8]Laboratory of Pharmaceutical Biotechnology, Department of Pharmaceutics, Ghent University, Ghent, Belgium; [9]NXTGNT, Ghent University, Ghent, Belgium and [10]OncoRNALab, Department of Biomolecular Medicine, Ghent University, Ghent, Belgium

** BP and NDS contributed equally as first authors.*

[#] PM, PN, KM-W and PVV contributed equally as senior authors.

[†]Deceased.

Correspondence: K. Matlawska-Wasowska
kmatlawska@uab.edu

P. Ntziachristos
panagiotis.ntziachristos@ugent.be

P. Mestdagh
pieter.mestdagh@ugent.be

B. Palhais
bruno.palhais@ugent.be

Received: March 25, 2025.
Accepted: December 30, 2025.
Early view: January 15, 2026.

https://doi.org/10.3324/haematol.2025.287809

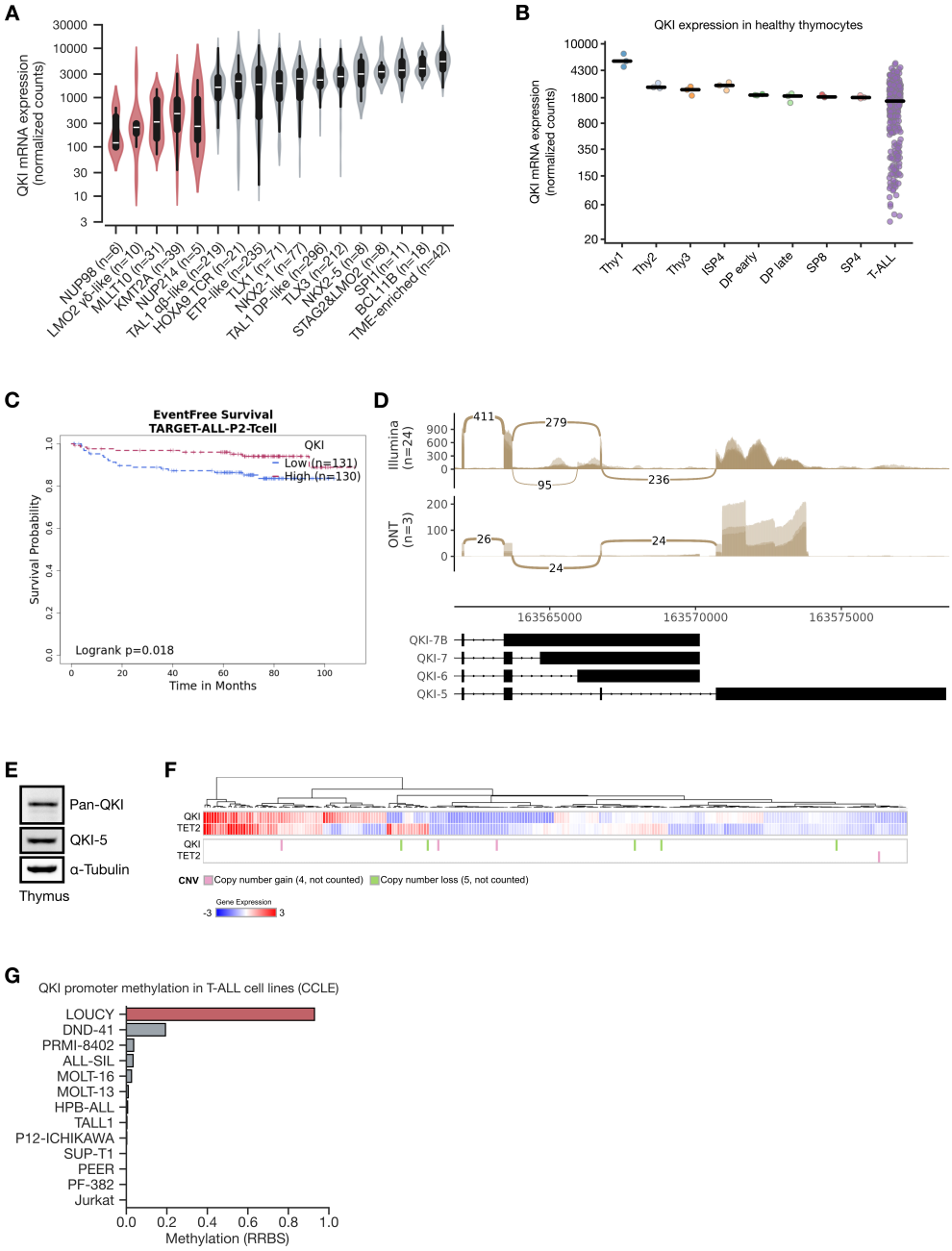

Supplementary Figure. 1: Analysis of *QKI* expression and genetic alterations in T-ALL and healthy thymocytes. (A) *QKI* mRNA expression across molecular subtypes from the Pölönen et al. (Nature 2024) cohort, showing subtype-specific variation. (B) *QKI* expression levels across different stages of thymocyte development (Thy1, Thy2, Thy3, ISP4, DP early, DP late, SP8, SP4), showing that *QKI* levels remains relatively constant in healthy thymocytes compared to T-ALL patient samples. (C) Kaplan-Meier plot displaying event free survival of T-ALL patients (TARGET) stratified into QKI-low and QKI-high. (D) Sashimi plots representing the splicing pattern of *QKI* using short-read sequencing (Illumina) from 24 healthy thymi samples and long-read sequencing (ONT) from 3 healthy thymi samples. The unique C-terminal end of each *QKI* isoform is shown below. Both sequencing technologies support the expression of QKI-5 as the main isoform, with QKI-6 detected to a much lesser extent only with short-read sequencing. (E) Western blot of QKI isoforms in a healthy thymus sample, using QKI-5, Pan-QKI and α-Tubulin as loading controls. (F) A heatmap illustrating *QKI* and *TET2* gene expression in T-ALL patient samples, highlighting similar expression patterns between the two genes across various patients. Below is copy number variation (CNV) and mutational burden analysis, showing instances of copy number gains and losses for *QKI* and *TET2* in T-ALL samples. (G) Bar plot depicting the levels of QKI promoter methylation, measured by reduced representation bisulfite sequencing (RRBS), across various T-ALL cell lines from the Cancer Cell Line Encyclopedia (CCLE).

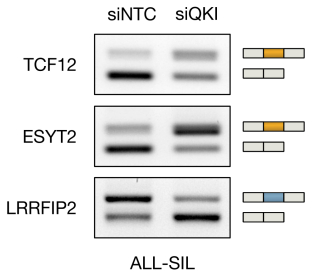

Supplementary Figure. 2: RT-PCR validation of QKI-dependent splicing events in ALL-SIL cells transfected with siNTC (control) or siQKI. Exon inclusion was assessed for *TCF12*, *ESYT2*, and *LRRFIP2* transcripts. The results confirm that QKI knockdown leads to altered splicing patterns in these genes, consistent with RNA-seq data.

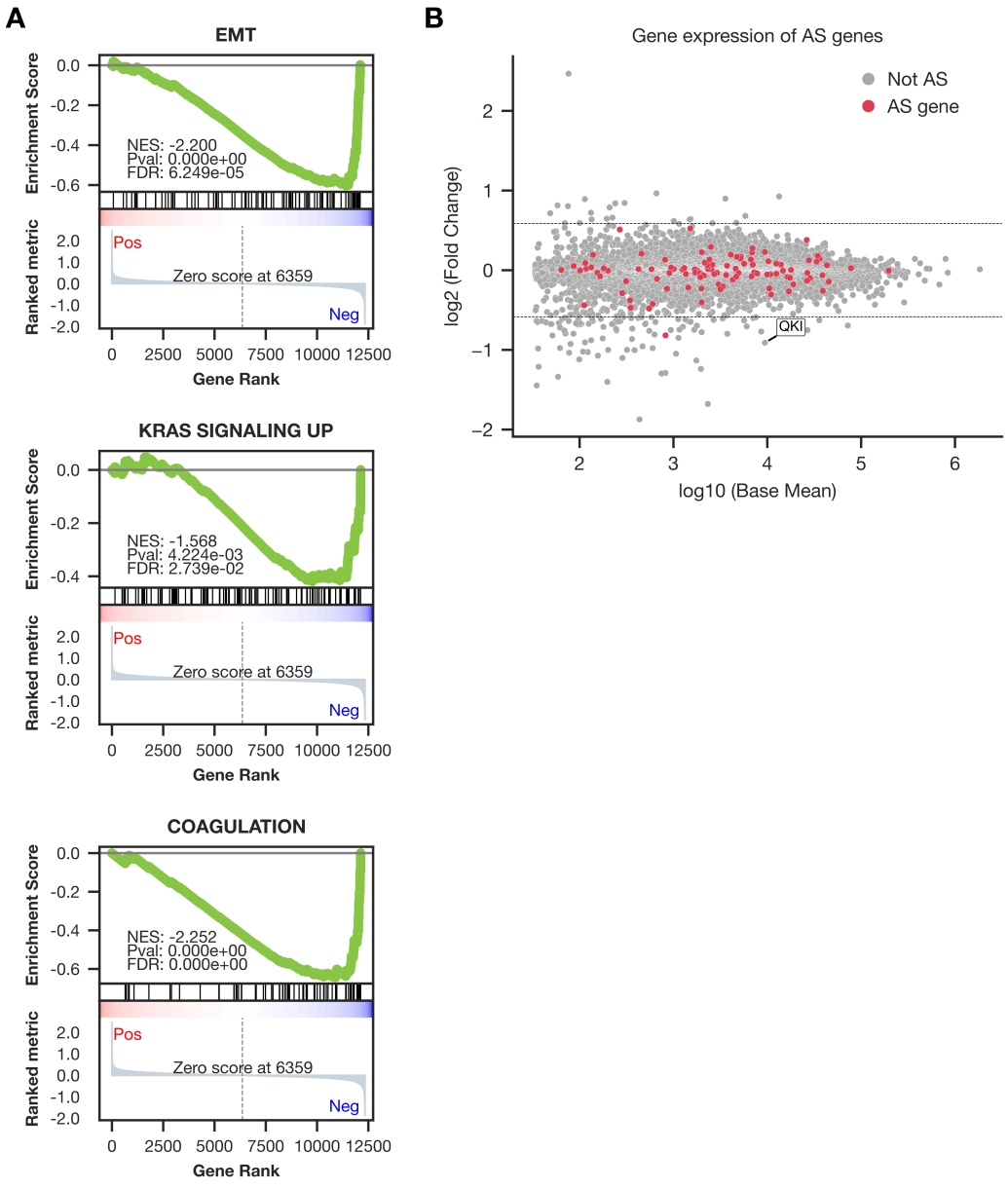

Supplementary Figure. 3: Gene set enrichment analysis (GSEA) and differential expression analysis following QKI silencing in HPB-ALL cells. (A) GSEA plots showing significant negative enrichment of hallmark gene sets for epithelial-mesenchymal transition (EMT), KRAS signaling up, and coagulation in QKI-depleted HPB-ALL cells. The normalized enrichment scores (NES), false discovery rates (FDR), and p-values indicate the significance of these pathway changes upon QKI silencing. (B) MA plot displaying the differential expression of genes following QKI knockdown. The plot highlights $\log_2$ fold changes relative to the mean expression across all genes. Alternatively spliced (AS) genes is marked in red, showcasing the relationship between differential splicing and expression changes.

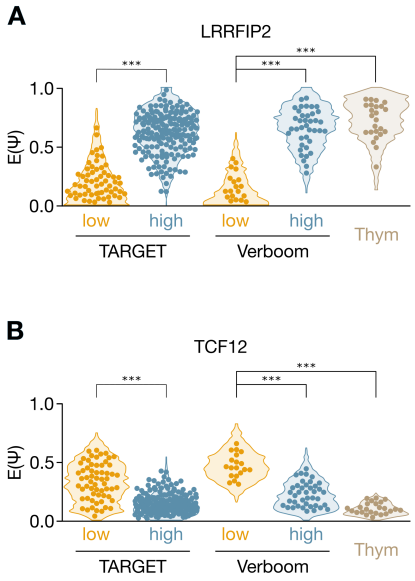

Supplementary Figure. 4: QKI-regulated splicing in *LRRFIP2* and *TCF12* across T-ALL cohorts and thymocytes. (A) Violin plots representing the expected percent spliced-in (E[Ψ]) values for the *LRRFIP2* alternative splicing event in the TARGET cohort (low vs. high expression groups) and the Verboom dataset (low vs. high expression groups), alongside thymocyte (Thym) samples as a reference. (B) Violin plots showing the E[Ψ] values for the *TCF12* alternative splicing event across the same cohorts and conditions. Statistical significance between groups was determined using the Mann-Whitney U test (***: $p < 0.001$).

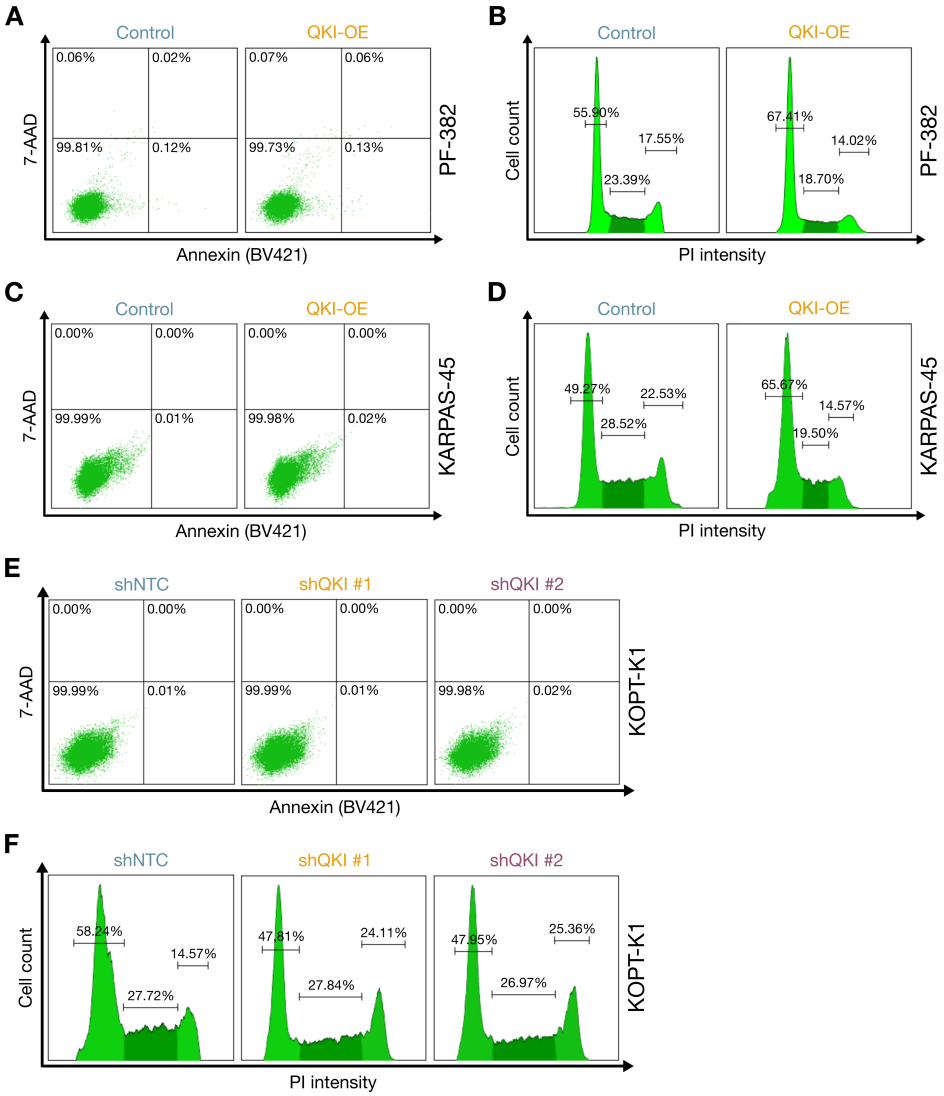

Supplementary Figure. 5: Apoptosis and cell-cycle analysis in QKI-overexpressing and QKI-depleted T-ALL cell lines. (A) Flow cytometry analysis of apoptosis in control and QKI-overexpressing (QKI-OE) PF-382 cells using Annexin V/7-AAD staining. The percentage of cells in early and late apoptosis is shown. No significant difference in apoptosis levels was observed between the two groups. (B) Cell cycle analysis of control and QKI-OE PF-382 cells by propidium iodide (PI) staining, showing an increased proportion of QKI-OE cells in the G0/G1 phase. (C) Annexin V/7-AAD staining of control and QKI-OE KARPAS-45 cells, showing no significant changes in apoptosis. (D) PI-based cell cycle analysis of KARPAS-45 cells, demonstrating a higher G0/G1 fraction in QKI-OE cells compared with controls. (E) Annexin V/7-AAD staining of KOPT-K1 cells transduced with non-targeting shRNA (shNTC) or QKI-targeting shRNAs (shQKI #1, shQKI #2), showing no increase in apoptosis upon QKI depletion. (F) PI-based cell cycle profiles of KOPT-K1 cells, showing reduced G0/G1 fractions in QKI-depleted cells compared with shNTC controls.

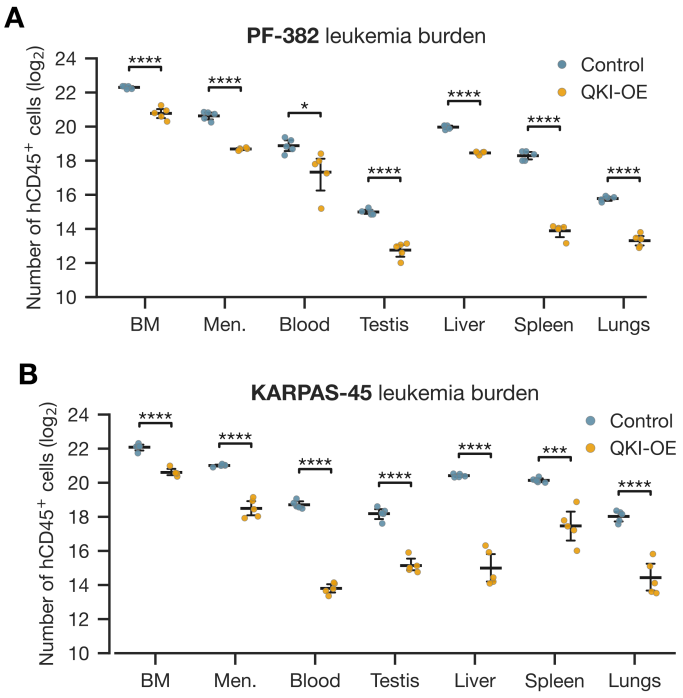

Supplementary Figure. 6: QKI overexpression prolongs survival in T-ALL xenografts. (A) Leukemia burden in NSG mice engrafted with PF-382 T-ALL cells (10^6 cell/mouse via tail vein) expressing either a control vector or QKI (QKI-OE) , quantified at Day 23 post-engraftment by the number of of human $CD45^+$ cells infiltrating bone marrow (BM), meninges (Men.), blood, testis, liver, spleen and lungs. (B) Leukemia burden in NSG mice engrafted with KARPAS-45 T-ALL cells expressing either control or QKI-OE, measured as in panel A. Statistical significance was determined using unpaired Student's t-test with Holm-Sidak multiple comparison correction (**: $p < 0.01$; ***: $p < 0.001$; ****: $p < 0.0001$).

Supplementary Material and Methods

QKI silencing in Jurkat and KOPT-K1 cells

Transfection was performed using the Neon transfection system (Thermo Fisher) and the device was set to 1325V, 10 ms, 3 pulses. Approximately $4x10^6$ cells were transfected with 20 nM of either an NTC or QKI siRNA (ON-TARGETplus SMARTpool siRNA; Dharmacon®). 72 hours post-transfection, total RNA was extracted and isolated using the RNeasy Plus mini kit (QIAGEN) according to manufacturer's instructions. The experiment was repeated 4 times. The two pre-designed shRNA targeting QKI (TR302174V) and a scrambled control (shNTC) (TR30021V) were purchased from Origene (Rockville, MD, USA). The sequences are: shQKI # 1: TTCAGTTACAAGAGAAACTTTATGTGCCT and shQKI # 2: ACTAATCACTGTGGAAGATGCTCAGAACA. The packaging vectors and recombinant expression plasmids were co-transfected into 293FT cells using Lipofectamine 2000 (Thermo Fisher Scientific). After 48 hours, viral supernatants were collected and titrated. Lentiviral particles were then mixed with 8 µg/ml Polybrene and applied to T-ALL cell lines at a multiplicity of infection (MOI) of 10. Following centrifugation, cells were selected with puromycin for approximately three weeks. GFP expression was analyzed on a FACSAria flow cytometer, and cells were sorted if the infection efficiency was below 85%.

QKI overexpression in KARPAS-45 and PF-382 cells

The recombinant expression plasmid Precision LentiORF QKI (QKI-OE) (OHS5900-202626095) and the corresponding control vector (OHS5833) were obtained from Dharmacon (Lafayette, CO, USA). Lentiviral packaging vectors pMD2.G, pMDLg/pRRE, and pRSV-Rev were purchased from Addgene (Cambridge, MA, USA). The transduction was performed as described above.

QKI knockdown in HPB-ALL

HEK293 cells were cotransfected with the envelope (pMD2.G), packaging (psPAX2) and the shRNA TRC vector (MISSION®) harboring either a non-targeting shRNA or an shRNA targeting QKI (TRCN0000233373). Viral particles were collected 72h and 96h post-transfection and concentrated 10 times using PEG-it (system biosciences). HPB-ALL cells were transduced with these viral particles by spinoculation (2300 rpm, 90 min, 32°C) in the presence of 8 µg/mL polybrene (Sigma, H9268). After 72 hours, 1 µg/mL of puromycin was included in the culturing media for the selection of transduced cells, for 7 days. Total RNA was extracted as above. The experiment was performed 4 times.

RT-qPCR

Reverse transcription was performed using iScript™ cDNA Synthesis Kit (BioRad) with 1 µg of RNA and input. qPCR was performed with the SsoAdvanced Universal SYBR® Green Supermix (BioRad, 1725275) under standard PCR conditions on a LightCycler® 480 System (Roche). The data was normalized and analyzed in the QBase+ software (CellCarta).

Cell viability assay

Cell viability was assessed using the CellTiter 96 AQueous One Solution Cell Proliferation Assay (MTS) (Promega, Madison, WI, USA). Using an Agilent BioTek 800 TS Microplate Absorbance Reader, the absorbance was measured at 490 nm.

Apoptosis and cell cycle

In 6-well plates, 10^6 T-ALL cells were cultured for 48 hours. Cells were washed in binding buffer and stained with 5 µl of Annexin V conjugated to BV421 and 5 µl of 7-ADD (BD Pharmingen, San Jose, CA, USA) for 15 minutes at RT in the dark. For cell cycle study, cells were frozen and permeable in 70% ethanol for 2 hours at -20°C. They were then treated with propidium iodide/RNase Staining Buffer (BD Pharmingen) for 15 minutes at RT. The stained cells were evaluated using flow cytometry and quantified using FlowJo software.